ELSEVIER

Comput. Methods Appl. Mech. Engrg. 190 (2000) 1529–1549

Computer methods in applied mechanics and engineering

www.elsevier.com/locate/cma

A finite element model for strain localization analysis of strongly discontinuous fields based on standard Galerkin approximation

Ronaldo I. Borja

Department of Civil and Environmental Engineering, Stanford University, Stanford, CA 94305, USA

Received 1 August 1999

Abstract

This paper presents a finite element model for strain localization analysis of elastoplastic solids subjected to discontinuous displacement fields based on standard Galerkin approximation. Strain enhancements via jumps in the displacement field are captured and condensed on the material level, leading to a formulation that does not require static condensation to be performed on the element level. The mathematical formulation revolves around the dual response of a macroscopic point cut by a shear band, which requires the satisfaction of the yield condition on the band as the same stress point unloads elastically just outside the band. Precise conditions for the appearance of slip lines, including their initiation and evolution, are outlined for a rate-independent, strain-softening Drucker–Prager model, and explicit analytical expressions are used to describe the orientation of the slip line in a plane strain setting. At post-localization the stress-point integration algorithm along the band is exact and amenable to consistent linearization. Numerical examples involving simple shearing of elastoplastic solids with deviatoric plastic flow, as well as plane strain compression of dilatant cohesive/frictional materials, are presented to demonstrate absolute objectivity with respect to mesh refinement and insensitivity to mesh alignment of finite element solutions.

1. Introduction

Strain localization is a ubiquitous feature of elastoplastic materials undergoing nonhomogeneous deformation. The phenomenon manifests in the form of a shear band, a narrow zone of intense straining across which some kinematical fields in a deforming body may be discontinuous. The formation of a shear band in a deforming body is accompanied by a softening response usually leading to complete collapse of the structure. Localized deformation is common in soils and rocks, materials that are susceptible to cracking and faulting when sheared [1–4]. It is also common in a variety of metals such as those exhibiting the so-called heat lines in the experimental work of Tresca [5].

Predictions of the formation of shear bands depend on the assumed material behavior. A classical approach consists of the bifurcation of a homogeneous solution into one involving a discontinuous deformation gradient [6–8], termed 'weak discontinuity' in [9]. The analysis identifies the loss of strong ellipticity of the governing equations of equilibrium, and signals the appearance of discontinuous solutions. Unfortunately, classical rate-independent plasticity models do not possess an intrinsic characteristic length scale that allows continuation of the analysis beyond the point of bifurcation. Consequently, less standard and usually more elaborate analysis approaches have been developed in conjunction with the weak discontinuity assumption to allow continuation of the solution beyond the point of bifurcation. Examples of nonconventional numerical approaches include the use of nonlocal constitutive models [10–13] as well as those developed from the idea of viscoplastic regularization [14,15].

0045-7825/00/$ - see front matter
PII: S0045-7825(00)00176-6

An alternative idea to the analysis of strain localization in elastoplastic solids has been advanced fairly recently and involves the assumption of a discontinuous displacement field, termed 'strong discontinuity' in [9]. The idea is equivalent to the assumption of a zero band thickness so that the constitutive model is no longer required to provide a characteristic length scale. As pointed out in [16], this assumption has some strong physical justifications for geologic materials, and was in fact central to the development of Coulomb's [17] and Rankine's [18] methods for earth pressure calculation, as well as to the development of the many bearing capacity and slope stability methods of analyses used in geotechnical applications [19–22]. Recent articles revolving around the idea of strong discontinuity for bifurcation analysis via the finite element method may be found in [9,16,23–28], among others.

Within the context of finite element analysis, the mathematical challenge imposed by the presence of a strongly discontinuous field has been met with satisfactory results by the introduction of an artificial enhancement to the element shape functions. The general approach falls within the framework of assumed enhanced strain methods described in [29] in which the kinematics of strong discontinuity is resolved by the introduction of an artificial jump parameter into the conforming displacement field, and then augmenting the standard weak equation for balance of momentum with an auxiliary equation, which imposes weakly the jump condition. Thus, the jump parameter becomes an artifact of the solution and is eliminated on the element level by static condensation. This approach has been tested with good results for deviatoric plasticity models with a constant post-localization softening modulus [9,23–25].

An extension of the enhanced strain formulation to a nonassociated Drucker–Prager plasticity model has been presented recently in [16] and incorporates the influence of dilatancy. In this work, it was shown that the auxiliary weak equation imposing the jump condition must be constructed consistently to capture the yield condition on the band. This results in an auxiliary weak equation that is dependent on the stress state, which renders the static condensation technique complicated from a numerical implementation standpoint. The technique also requires stress-point integration of the auxiliary weak equation to be performed at post-localization, which could introduce additional numerical errors.

This paper presents a reformulation of the theory presented in [16], as well as those formulated based on the assumed enhanced strain methods [9,23–28], within the setting provided by the standard Galerkin approximation. The idea is to consider the post-localization response of a damaged element as no more than a classical plasticity problem except that yielding is now localized to the band. Following the development of [16], the auxiliary weak equation is now interpreted as nothing else but the consistency condition on the band, while the jump parameter now takes the role of the consistency parameter. The advantage of the new formulation is that the consistency parameter is now eliminated on the material level, thus rendering the auxiliary weak equation redundant and completely unnecessary. For the case of simple triangulation using constant strain triangle elements, the method advocated in this paper is shown to be equivalent to that based on the assumed enhanced strain method presented in [16].

In the post-localization regime the stress-point integration used for the damaged elements is exact regardless of the yield condition, as well as amenable to consistent linearization. Like the method presented in [16], the formulation satisfies both the localization and evolution conditions, which require that the traction vector be continuous across the band during and following localization. The method is tested for elastoplastic solids with deviatoric plastic flow (von Mises model), as well as for dilatant cohesive/frictional materials (nonassociated Drucker–Prager model). Numerical examples demonstrate that the finite element solutions are objective with respect to mesh refinement and insensitive to mesh alignment.

As for notations and symbols, bold-face letters denote matrices and vectors; the symbol '$\cdot$' denotes an inner product of two vectors (e.g., $\boldsymbol{a} \cdot \boldsymbol{b} = a_i b_i$), or a single contraction of adjacent indices of two tensors (e.g., $\boldsymbol{c} \cdot \boldsymbol{d} = c_{ij} d_{jk}$); the symbol ':' denotes an inner product of two second-order tensors (e.g., $\boldsymbol{c} : \boldsymbol{d} = c_{ij} d_{ij}$), or a double contraction of adjacent indices of tensors of rank two and higher (e.g., $\boldsymbol{C} : \boldsymbol{\epsilon}^{\mathrm{e}} = C_{ijkl} \epsilon^{\mathrm{e}}_{kl}$).

2. Framework for nonassociated plasticity with strongly discontinuous fields

The model problem we want to address concerns a slip surface $\mathscr{S}$ in a body Ω across which the displacement field $\boldsymbol{u}$ is discontinuous. The slip surface, or band, is defined by a unit normal vector $\boldsymbol{n}$ which could vary from point to point on $\mathscr{S}$. We assume that $\boldsymbol{u}$ varies according to the equation

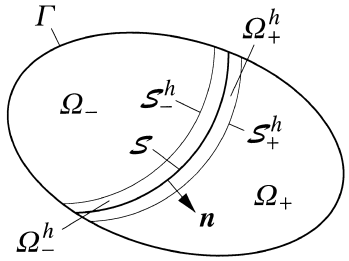

Fig. 1. Definition of surface of discontinuity.

$$\boldsymbol{u} = \bar{\boldsymbol{u}} + [\![\boldsymbol{u}]\!] H_{\mathscr{S}}(\boldsymbol{x}), \qquad H_{\mathscr{S}}(\boldsymbol{x}) = \begin{cases} 1 & \text{if } \boldsymbol{x} \in \Omega_+, \\ 0 & \text{if } \boldsymbol{x} \in \Omega_-, \end{cases} \tag{2.1}$$

where $\bar{\boldsymbol{u}}$ is the continuous part of $\boldsymbol{u}$, and $[\![\boldsymbol{u}]\!]$ is the jump discontinuity on the surface $\mathscr{S}$ separating the subdomains Ω_+ and Ω_- of Ω, see Fig. 1.

Additional assumptions are necessary to fully describe the kinematics of displacement jump. First, we assume that the displacement gradients just in front of the band are the same as those immediately behind it, although they may be separated by the delta function because of the displacement jump. For the infinitesimal case, this is satisfied by the evolution condition [16] that the continuum stresses $\boldsymbol{\sigma}$ remain continuous across the surface of discontinuity. Furthermore, we assume that the jump discontinuity $[\![\boldsymbol{u}]\!]$ is relatively uniform in Ω_+ so that the gradient $\nabla[\![\boldsymbol{u}]\!]$ may be ignored. If this is not the case, then we can always construct a uniform jump function $[\![\boldsymbol{u}]\!]$ in Ω_+ by requiring the continuous component $\bar{\boldsymbol{u}}$ to take in the nonuniform part, provided of course that $[\![\boldsymbol{u}]\!]$ itself is relatively uniform along $\mathscr{S}$. In this case, the associated total strain rate tensor resulting from (2.1) is the symmetric component of the displacement gradient tensor $\nabla\boldsymbol{u}$, which can be written in a compact form as [9]

$$\dot{\boldsymbol{\epsilon}} = \mathrm{sym}(\nabla\dot{\boldsymbol{u}}) + \mathrm{sym}([\![\dot{\boldsymbol{u}}]\!] \otimes \boldsymbol{n}\delta_{\mathscr{S}}), \tag{2.2}$$

where $\delta_{\mathscr{S}}$ is the Dirac delta function on the surface $\mathscr{S}$. A one-dimensional representation of the variation of $\boldsymbol{u}$ with $\boldsymbol{x}$ is shown in Fig. 2.

2.1. Constitutive model in the presence of displacement jump

Adopting the same terminologies and notations used in [9], we consider a convex elastic domain $\boldsymbol{E}'$ defined by a smooth yield function $\mathscr{G}$ characterizing the yield condition on the band

$$\boldsymbol{E}' = \{(\boldsymbol{\sigma}, \boldsymbol{\phi}) \in S \times R^n \mid \mathscr{G}(\boldsymbol{\sigma}, \boldsymbol{\phi}) \leqslant 0\}, \tag{2.3}$$

where S is the space of symmetric rank-two tensors, and $\boldsymbol{\phi}$ is a stress-like vector of plastic internal variables of dimension n characterizing the softening response of the band. Note that $\mathscr{G}$ is not necessarily the same as

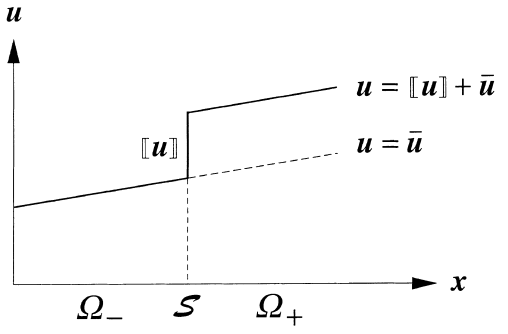

Fig. 2. Graphical representation of displacement jump.

the yield function $\mathscr{F}$, which describes the yield condition for an intact continuum. In addition, we assume a nonassociated model and consider a plastic potential function $\mathscr{R} \neq \mathscr{G}$ describing the irreversible deformation response of the material on the band. Although the function $\mathscr{R}$ is used to describe plastic yielding on the band, the model does not in fact require an explicit form for this function, as elaborated in [16] and reiterated further in the following discussions.

Yielding in the damaged state is described by the consistency condition [16]

$$\dot{\mathscr{G}}(\boldsymbol{\sigma}, \boldsymbol{\phi}) = \frac{\partial \mathscr{G}}{\partial \boldsymbol{\sigma}} : \dot{\boldsymbol{\sigma}} - \lambda \bar{\mathscr{H}} = 0, \tag{2.4}$$

where $\dot{\boldsymbol{\sigma}}$ is the stress rate tensor which takes the form

$$\dot{\boldsymbol{\sigma}} = \boldsymbol{c}^{\mathrm{e}} : (\dot{\boldsymbol{\epsilon}} - \dot{\boldsymbol{\epsilon}}^{\mathrm{p}}) = \boldsymbol{c}^{\mathrm{e}} : \left[\mathrm{sym}(\nabla \dot{\boldsymbol{u}}) + \mathrm{sym}(\llbracket \dot{\boldsymbol{u}} \rrbracket \otimes \boldsymbol{n} \delta_{\mathscr{S}}) - \lambda \frac{\partial \mathscr{R}}{\partial \boldsymbol{\sigma}} \right], \tag{2.5}$$

where $\bar{\mathscr{H}}$ is the softening modulus on the band, $\boldsymbol{c}^{\mathrm{e}}$ the rank-four tensor of elastic moduli, and $\lambda \geqslant 0$ is the usual plastic consistency parameter. Assuming that plasticity is localized to the discontinuity, we can use theory of distribution [30] and write λ and $\bar{\mathscr{H}}$ in terms of the distribution functions [9,23]

$$\lambda = \lambda_\delta \delta_{\mathscr{S}}, \qquad \bar{\mathscr{H}}^{-1} = \mathscr{H}_\delta^{-1} \delta_{\mathscr{S}}. \tag{2.6}$$

Thus, (2.4) and (2.5) imply the two separate conditions

$$\frac{\partial \mathscr{G}}{\partial \boldsymbol{\sigma}} : \boldsymbol{c}^{\mathrm{e}} : \mathrm{sym}(\nabla \dot{\boldsymbol{u}}) - \lambda_\delta \mathscr{H}_\delta = 0 \tag{2.7}$$

for the regular part, and

$$\frac{\partial \mathscr{G}}{\partial \boldsymbol{\sigma}} : \boldsymbol{c}^{\mathrm{e}} : \left[\mathrm{sym}(\llbracket \dot{\boldsymbol{u}} \rrbracket \otimes \boldsymbol{n}) - \lambda_\delta \frac{\partial \mathscr{R}}{\partial \boldsymbol{\sigma}} \right] = 0 \tag{2.8}$$

for the singular part. Since $\lambda_\delta \mathscr{H}_\delta < 0$, by definition, then (2.7) gives $\partial \mathscr{G} / \partial \boldsymbol{\sigma} : \boldsymbol{c}^{\mathrm{e}} : \mathrm{sym}(\nabla \dot{\boldsymbol{u}}) < 0$, thus effectively capturing the softening response.

The assumption that plasticity is localized to the discontinuity implies that the slip rate tensor $\mathrm{sym}(\llbracket \dot{\boldsymbol{u}} \rrbracket \otimes \boldsymbol{n})$ is fully plastic, and so we can write

$$\mathrm{sym}(\llbracket \dot{\boldsymbol{u}} \rrbracket \otimes \boldsymbol{n}) = \lambda_\delta \frac{\partial \mathscr{R}}{\partial \boldsymbol{\sigma}}. \tag{2.9}$$

This automatically satisfies the requirement that the singular component of the consistency condition must vanish (see (2.8)), so that the stress rate tensor $\dot{\boldsymbol{\sigma}}$ simply becomes

$$\dot{\boldsymbol{\sigma}} = \boldsymbol{c}^{\mathrm{e}} : (\dot{\boldsymbol{\epsilon}} - \dot{\boldsymbol{\epsilon}}^{\mathrm{p}}) = \boldsymbol{c}^{\mathrm{e}} : \mathrm{sym}(\nabla \dot{\boldsymbol{u}}). \tag{2.10}$$

Thus, $\dot{\boldsymbol{\sigma}}$ depends solely on the regular component of the total strain rate.

It is more meaningful to express λ_δ in terms of the magnitude $\dot{\zeta}$ of the slip rate vector $\llbracket \dot{\boldsymbol{u}} \rrbracket$, which is defined in the sense that $\llbracket \dot{\boldsymbol{u}} \rrbracket = \dot{\zeta} \boldsymbol{m}$, where $\boldsymbol{m}$ is the unit vector in the direction of $\llbracket \dot{\boldsymbol{u}} \rrbracket$. In this case, (2.9) can be written as

$$\mathrm{sym}(\boldsymbol{m} \otimes \boldsymbol{n}) = \Lambda \frac{\partial \mathscr{R}}{\partial \boldsymbol{\sigma}}, \quad \Lambda = \lambda_\delta / \dot{\zeta}, \tag{2.11}$$

which implies that the real component λ_δ is a linear measure of $\dot{\zeta}$. Thus, (2.7) can also be written in the form

$$\frac{\partial \mathscr{G}}{\partial \boldsymbol{\sigma}} : \dot{\boldsymbol{\sigma}} - \tilde{\mathscr{H}}_\delta \dot{\zeta} = 0, \tag{2.12}$$

where $\tilde{\mathscr{H}}_\delta$ is an alternative softening modulus on the band [16].

The developments described above are central to the formulation presented in [16] and demonstrate the dual nature of the response of a macroscopic point intersected by a slip surface. Eq. (2.10) describes the

evolution of the stress rate just outside the band and reflects the elastic unloading that takes place in the continuum arising from assumption (2.11), i.e., that plasticity is localized to the surface of discontinuity. Relation (2.12) is the consistency condition on the band, which, in conjunction with (2.10) for the stress rate, implies that the stresses on the band are the same as those just outside the band. In the following section, we present a finite element model based on the standard Galerkin method that effectively captures this dual response of a damaged continuum.

2.2. Finite element formulation

For simplicity, the discussions that follow will be restricted to quasi-static loading under the assumption of infinitesimal deformation. In this case, the finite element approximations are based on the standard weak equation

$$\int_\Omega \mathrm{sym}(\nabla\boldsymbol{\eta}) : \dot{\boldsymbol{\sigma}}\, \mathrm{d}\Omega = \int_\Omega \boldsymbol{\eta}\cdot\dot{\boldsymbol{f}}\, \mathrm{d}\Omega + \int_\Gamma \boldsymbol{\eta}\cdot\dot{\boldsymbol{t}}\, \mathrm{d}\Gamma, \tag{2.13}$$

where $\mathrm{sym}(\nabla\boldsymbol{\eta})$ represents the compatible component of the total strain variation, $\boldsymbol{f}$ is the body force vector, and $\boldsymbol{t}$ is the traction vector. For a body Ω intersected by a band, it can be demonstrated [23] that the weak equation presented above is equivalent to a pointwise satisfaction of the local equilibrium equations

$$\mathrm{div}(\dot{\boldsymbol{\sigma}}) + \dot{\boldsymbol{f}} = \boldsymbol{0} \quad \text{in } \Omega\setminus\mathscr{S} \tag{2.14a}$$

$$\boldsymbol{v}\cdot\dot{\boldsymbol{\sigma}} = \dot{\boldsymbol{t}} \quad \text{on } \Gamma_t \tag{2.14b}$$

and supplemented with the additional conditions

$$\boldsymbol{n}\cdot\dot{\boldsymbol{\sigma}}_{\mathscr{S}} = \boldsymbol{n}\cdot\dot{\boldsymbol{\sigma}}_+ = \boldsymbol{n}\cdot\dot{\boldsymbol{\sigma}}_-, \tag{2.14c}$$

where $\boldsymbol{v}$ is the outward unit normal vector to Γ_t, $\boldsymbol{n}$ the unit normal vector to $\mathscr{S}$ and pointing toward Ω_+, and $\boldsymbol{\sigma}_{\mathscr{S}}$, $\boldsymbol{\sigma}_-$, and $\boldsymbol{\sigma}_+$ are the stresses on the band, behind the band, and in front of the band, respectively. Condition (2.14c) simply requires that the traction vector be continuous across the band.

Now consider a localized element Ω^e intersected by a band. To incorporate the constraint imposed by the presence of a discontinuous displacement field, let us write the velocity vector $\dot{\boldsymbol{u}}$ in the reparameterized form

$$\dot{\boldsymbol{u}} = \dot{\tilde{\boldsymbol{u}}} + [\![\dot{\boldsymbol{u}}]\!] M_{\mathscr{S}}. \tag{2.15}$$

Here, the jump of $M_{\mathscr{S}}$ across $\mathscr{S}$ is $[\![M_{\mathscr{S}}]\!] = 1$, with $M_{\mathscr{S}} = 0$ on the surface $\mathscr{S}^h_\pm$ of its (compact) support Ω^h, as shown in Fig. 1. A comparison of (2.15) with (2.1) suggests that $\dot{\tilde{\boldsymbol{u}}} = \dot{\bar{\boldsymbol{u}}}$ in $\Omega_-\setminus\Omega^h_-$, and $\dot{\tilde{\boldsymbol{u}}} = \dot{\bar{\boldsymbol{u}}} + [\![\dot{\boldsymbol{u}}]\!]$ in $\Omega_+\setminus\Omega^h_+$, and so $\tilde{\boldsymbol{u}}$ simply describes the total motion of the continuum including the jump discontinuity $[\![\boldsymbol{u}]\!]$. In terms of the Heaviside function $H_{\mathscr{S}}$, the jump function $M_{\mathscr{S}}$ may be represented as

$$M_{\mathscr{S}} = H_{\mathscr{S}} - f^h, \tag{2.16}$$

where f^h is any arbitrary smooth ramp function that satisfies the requirement that $f^h = 0$ in $\Omega_-\setminus\Omega^h_-$, and $f^h = 1$ in $\Omega_+\setminus\Omega^h_+$.

As before, we obtain the associated total strain rate tensor resulting from the reparameterized velocity field (2.15) from the symmetric component of the velocity gradient tensor, which is now written as

$$\dot{\boldsymbol{\epsilon}} = \mathrm{sym}(\nabla\dot{\tilde{\boldsymbol{u}}}) - \dot{\zeta}\,\mathrm{sym}(\nabla f^h\otimes\boldsymbol{m}) + \dot{\zeta}\,\mathrm{sym}(\boldsymbol{n}\otimes\boldsymbol{m})\delta_{\mathscr{S}}. \tag{2.17}$$

In (2.17), use was made again of theory of distribution as well as of the assumption that $\nabla[\![\dot{\boldsymbol{u}}]\!]$ is negligible.

The elastic component of $\dot{\boldsymbol{\epsilon}}$ can be determined by subtracting its plastic part, which is obtained from the flow rule as

$$\dot{\boldsymbol{\epsilon}}^{\mathrm{e}} = \mathrm{sym}(\nabla\dot{\tilde{\boldsymbol{u}}}) - \dot{\zeta}\,\mathrm{sym}(\nabla f^h\otimes\boldsymbol{m}) + \dot{\zeta}\,\mathrm{sym}(\boldsymbol{n}\otimes\boldsymbol{m})\delta_{\mathscr{S}} - \lambda_\delta\delta_{\mathscr{S}}\frac{\partial\mathscr{R}}{\partial\boldsymbol{\sigma}}. \tag{2.18}$$

Recall that the delta function appearing in the last term of (2.18) arises from the assumption that plasticity is localized to the discontinuity and so (2.9) holds. Thus, the last two terms of (2.18) cancel, and so the rate-constitutive equation becomes

$$\dot{\boldsymbol{\sigma}} = \boldsymbol{c}^{\mathrm{e}} : \dot{\boldsymbol{\epsilon}}^{\mathrm{e}} = \dot{\boldsymbol{\sigma}}^{\mathrm{tr}} - \dot{\zeta}\boldsymbol{c}^{\mathrm{e}} : \mathrm{sym}(\nabla f^h \otimes \boldsymbol{m}), \tag{2.19}$$

where $\dot{\boldsymbol{\sigma}}^{\mathrm{tr}} = \boldsymbol{c}^{\mathrm{e}} : \mathrm{sym}(\nabla \dot{\tilde{\boldsymbol{u}}})$ is the trial rate of stress.

Remark 1. Eq. (2.19) follows the format of standard continuum plasticity theory in that the stress rate is computed as the difference between an elastic stress predictor evaluated from the total motion $\tilde{\boldsymbol{u}}$ and a plastic stress corrector resulting from the jump rate $\dot{\zeta}$. In the presence of displacement jumps, $\dot{\zeta} \geqslant 0$ serves to take the role of the consistency parameter of continuum plasticity theory. However, since the jump is localized to the discontinuity, the ramp function f^h is introduced to "release" the effect of the concentrated displacement jump into the neighboring continuum. Note that f^h is not meant to approximate the Heaviside function $H_{\mathscr{S}}$ since an appropriate function $M_{\mathscr{S}}$ can always be combined with whatever one chooses for the function f^h to obtain $H_{\mathscr{S}}$, as shown in (2.16). As we will show later in the next section, the function f^h plays an important role in developing a mesh-independent finite element solution to the problem of strain localization with displacement jumps.

Let us now impose the consistency condition on the band. From (2.12), we have

$$\boldsymbol{\psi} : \dot{\boldsymbol{\sigma}} - \tilde{\mathscr{H}}_\delta \dot{\zeta} = 0, \quad \boldsymbol{\psi} = \frac{\partial \mathscr{G}}{\partial \boldsymbol{\sigma}}. \tag{2.20}$$

Substituting (2.19) into (2.20) and solving for the consistency parameter gives

$$\dot{\zeta} = \frac{\boldsymbol{\psi} : \dot{\boldsymbol{\sigma}}^{\mathrm{tr}}}{\boldsymbol{\psi} : \boldsymbol{c}^{\mathrm{e}} : \mathrm{sym}(\nabla f^h \otimes \boldsymbol{m}) + \tilde{\mathscr{H}}_\delta}. \tag{2.21}$$

Substituting back to (2.19) gives

$$\dot{\boldsymbol{\sigma}} = \tilde{\boldsymbol{c}}^{\mathrm{ep}} : \mathrm{sym}(\nabla \dot{\tilde{\boldsymbol{u}}}), \tag{2.22}$$

where $\tilde{\boldsymbol{c}}^{\mathrm{ep}}$ is an equivalent elastoplastic tangential moduli tensor which takes the form

$$\tilde{\boldsymbol{c}}^{\mathrm{ep}} = \boldsymbol{c}^{\mathrm{e}} - \tilde{\boldsymbol{c}}^{\mathrm{p}}, \quad \tilde{\boldsymbol{c}}^{\mathrm{p}} = \frac{\boldsymbol{c}^{\mathrm{e}} : \mathrm{sym}(\nabla f^h \otimes \boldsymbol{m}) \otimes \boldsymbol{\psi} : \boldsymbol{c}^{\mathrm{e}}}{\boldsymbol{\psi} : \boldsymbol{c}^{\mathrm{e}} : \mathrm{sym}(\nabla f^h \otimes \boldsymbol{m}) + \tilde{\mathscr{H}}_\delta}. \tag{2.23}$$

We can see that the component $\tilde{\boldsymbol{c}}^{\mathrm{p}}$ is responsible for the softening response of a localized element. For clarity, a tilde $\tilde{(\cdot)}$ is written over the tensors $\boldsymbol{c}^{\mathrm{ep}}$ and $\boldsymbol{c}^{\mathrm{p}}$ to distinguish them from the standard tangential moduli tensors used in continuum plasticity theory.

In order for (2.21) to be meaningful, the slip rate $\dot{\zeta}$ must be nonnegative. Now, since $\boldsymbol{\psi} : \dot{\boldsymbol{\sigma}}^{\mathrm{tr}} > 0$ defines a plastic process, and must be satisfied or there will be no yielding on the band, then $\dot{\zeta} > 0$ implies that

$$\chi := \boldsymbol{\psi} : \boldsymbol{c}^{\mathrm{e}} : \mathrm{sym}(\nabla f^h \otimes \boldsymbol{m}) + \tilde{\mathscr{H}}_\delta > 0. \tag{2.24}$$

Eq. (2.24) thus represents a constraint imposed on the ramp function f^h if the formulation is to provide a meaningful solution. Since $\tilde{\mathscr{H}}_\delta < 0$ in order for a bifurcated solution to be possible, then $\boldsymbol{\psi} : \boldsymbol{c}^{\mathrm{e}} : \mathrm{sym}(\nabla f^h \otimes \boldsymbol{m})$ itself must be positive and must be greater than $-\tilde{\mathscr{H}}_\delta$ in order for (2.24) to be satisfied. Eq. (2.24) can thus be used to determine the most negative value of the softening modulus $\tilde{\mathscr{H}}_\delta$ for the solution of (2.21) to be meaningful.

The finite element matrix equation can be developed following standard lines. Letting Ω^e denote the domain of any localized element e, the element matrix equation becomes

$$\int_{\Omega^e} \boldsymbol{B}^{\mathrm{t}} \tilde{\boldsymbol{D}}^{\mathrm{ep}} \boldsymbol{B} \, \mathrm{d}\Omega^e \dot{\boldsymbol{d}}^e = \int_{\Omega^e} \boldsymbol{N}^{\mathrm{t}} \dot{\boldsymbol{f}} \, \mathrm{d}\Omega^e + \int_{\Gamma^e} \boldsymbol{N}^{\mathrm{t}} \dot{\boldsymbol{t}} \, \mathrm{d}\Gamma^e, \tag{2.25}$$

where $\tilde{\boldsymbol{D}}^{\mathrm{ep}}$ is the matrix counterpart of $\tilde{\boldsymbol{c}}^{\mathrm{ep}}$. Since the interpolation is based on the total motion $\tilde{\boldsymbol{u}}$, the vector $\boldsymbol{d}^e$ has the physical significance of being the total element nodal displacement vector, and therefore includes the effect of the displacement jump.

2.3. Equivalence of standard Galerkin and assumed enhanced strain approximations

In this section we demonstrate the equivalence between the formulation presented in Section 2.2 and the assumed enhanced strain finite element formulation presented in [16] for the case of piecewise constant stress field approximation. For purposes of completeness, we recall the following finite element approximations arising from the assumed enhanced strain method [29]:

$$\int_{\Omega^e} \mathrm{sym}(\nabla \bar{\boldsymbol{\eta}}^h) : \dot{\boldsymbol{\sigma}} \, \mathrm{d}\Omega^e = \int_{\Omega^e} \bar{\boldsymbol{\eta}}^h \cdot \dot{\boldsymbol{f}} \, \mathrm{d}\Omega^e + \int_{\Gamma^e} \bar{\boldsymbol{\eta}}^h \cdot \dot{\boldsymbol{t}} \, \mathrm{d}\Gamma^e, \tag{2.26a}$$

$$\int_{\Omega^e} \tilde{\boldsymbol{\gamma}}^h : \dot{\boldsymbol{\sigma}} \, \mathrm{d}\Omega^e = 0 \quad \forall e \in \{\text{set of localized elements}\}, \tag{2.26b}$$

where $\mathrm{sym}(\nabla \bar{\boldsymbol{\eta}}^h)$ represents the compatible component of the total strain variation, $\tilde{\boldsymbol{\gamma}}^h$ represents the assumed enhanced component, and Ω^e is the domain of any localized element. Eq. (2.26a) is the usual weak statement of balance of momentum, while (2.26b) defines the nature of the enhancement for the localized elements. In order to enhance the compatible strain field, the spaces of the weighting functions $\tilde{\boldsymbol{\gamma}}^h$ and $\mathrm{sym}(\nabla \bar{\boldsymbol{\eta}}^h)$ are required to have a null intersection [29].

The particular case where the displacement jump is not equal to zero requires the construction of the weighting function $\tilde{\boldsymbol{\gamma}}^h$ for use in the weak Eq. (2.26b). This is facilited by a function of the form [16]

$$\tilde{\boldsymbol{\gamma}}^h = \xi \left[\frac{\ell^e_{\mathscr{S}}}{A_e} \boldsymbol{\psi} - \boldsymbol{\psi} \delta_{\mathscr{S}} \right], \quad \boldsymbol{\psi} = \frac{\partial \mathscr{G}}{\partial \boldsymbol{\sigma}}, \quad \xi \in R^1, \tag{2.27}$$

where A_e is the area of the localized element Ω^e, and $\ell^e_{\mathscr{S}}$ is the length of the discontinuity line. This weighting function has a null intersection with $\mathrm{sym}(\nabla \bar{\boldsymbol{\eta}}^h)$, and satisfies the stability and consistency (patch test) conditions set forth in [29] for convergence of enhanced strain methods.

Substituting (2.27) in (2.26b) and taking note that ξ is an arbitrary nonzero scalar function gives

$$\frac{\ell^e_{\mathscr{S}}}{A^e} \int_{\Omega^e} \boldsymbol{\psi} : \dot{\boldsymbol{\sigma}} \, \mathrm{d}\Omega^e = \int_{\mathscr{S}^e} \boldsymbol{\psi} : \dot{\boldsymbol{\sigma}} \, \mathrm{d}\mathscr{S}^e = \ell^e_{\mathscr{S}} \boldsymbol{\psi} : \dot{\boldsymbol{\sigma}}, \tag{2.28}$$

assuming that $\boldsymbol{\psi} : \dot{\boldsymbol{\sigma}}$ is constant along $\mathscr{S}^e$. Thus, from (2.20) we get

$$\int_{\Omega^e} \boldsymbol{\psi} : \dot{\boldsymbol{\sigma}} \, \mathrm{d}\Omega^e - \int_{\Omega^e} \tilde{\mathscr{H}}_\delta \dot{\zeta}^e \, \mathrm{d}\Omega^e = 0. \tag{2.29}$$

where $\dot{\zeta}^e$ is the slip rate on the band associated with localized element e. For clarity, we recall that the conventional procedure allows for the slip rate $\dot{\zeta}^e$ to be piecewise constant for each localized element and therefore is discontinuous across the element boundaries. Thus, with a suitable choice of the weighting function for the element enhancement, we recover precisely the consistency condition on the band.

Consider now the matrix form of the boundary value problem obtained by making the substitutions

$$\bar{\boldsymbol{\eta}}^h \to \boldsymbol{N} \boldsymbol{\phi}^e, \quad \mathrm{sym}(\nabla \bar{\boldsymbol{\eta}}^h) \to \boldsymbol{B} \boldsymbol{\phi}^e, \quad \boldsymbol{\psi} \to \boldsymbol{F}, \ \mathrm{sym}(\nabla f^h_e \otimes \boldsymbol{m}) \to \boldsymbol{G}, \quad \boldsymbol{c}^{\mathrm{e}} \to \boldsymbol{D}^{\mathrm{e}}, \tag{2.30}$$

where $\boldsymbol{\phi}^e \in R^{n_{\mathrm{ed}}}$ is an arbitrary vector of nodal displacements, and n_{ed} is the number of element displacement degrees of freedom. With a slight abuse in notation, we will use the same symbol $\dot{\boldsymbol{\sigma}}$ to denote the stress rate tensor and the stress rate vector.

Substituting the constitutive Eq. (2.19) in Eqs. (2.26a) and (2.26b) gives

$$\boldsymbol{K}^e_{dd} \dot{\boldsymbol{d}}^e + \boldsymbol{K}^e_{d\zeta} \dot{\zeta}^e = \int_{\Omega^e} \boldsymbol{N}^{\mathrm{t}} \dot{\boldsymbol{f}} \, \mathrm{d}\Omega^e + \int_{\Gamma^e} \boldsymbol{N}^{\mathrm{t}} \dot{\boldsymbol{t}} \, \mathrm{d}\Gamma^e, \tag{2.31a}$$

$$\boldsymbol{K}^e_{\zeta d} \dot{\boldsymbol{d}}^e + K^e_{\zeta\zeta} \dot{\zeta}^e = 0, \tag{2.31b}$$

where

$$\boldsymbol{K}^e_{dd} = \int_{\Omega^e} \boldsymbol{B}^{\mathrm{t}} \boldsymbol{D}^{\mathrm{e}} \boldsymbol{B} \, \mathrm{d}\Omega^e, \quad \boldsymbol{K}^e_{d\zeta} = -\int_{\Omega^e} \boldsymbol{B}^{\mathrm{t}} \boldsymbol{D}^{\mathrm{e}} \boldsymbol{G} \, \mathrm{d}\Omega^e,$$

$$\boldsymbol{K}^e_{\zeta d} = \int_{\Omega^e} \boldsymbol{F}^{\mathrm{t}} \boldsymbol{D}^{\mathrm{e}} \boldsymbol{B}\, \mathrm{d}\Omega^e, \quad K^e_{\zeta\zeta} = -\int_{\Omega^e} \left(\boldsymbol{F}^{\mathrm{t}} \boldsymbol{D}^{\mathrm{e}} \boldsymbol{G} + \tilde{\mathscr{H}}_\delta \right) \mathrm{d}\Omega^e. \tag{2.32}$$

Since ζ^e is discontinuous across the element boundaries, the finite element matrix equations may be condensed statically to eliminate the slip rate term on the element level. The result reads

$$\tilde{\boldsymbol{K}} \dot{\boldsymbol{d}}^e = \int_{\Omega^e} \boldsymbol{N}^{\mathrm{t}} \dot{\boldsymbol{f}}\, \mathrm{d}\Omega^e + \int_{\Gamma^e} \boldsymbol{N}^{\mathrm{t}} \dot{\boldsymbol{t}}\, \mathrm{d}\Gamma^e, \tag{2.33}$$

where

$$\tilde{\boldsymbol{K}} = \boldsymbol{K}^e_{dd} - \tilde{\boldsymbol{K}}_{dd}, \quad \tilde{\boldsymbol{K}}_{dd} = \boldsymbol{K}_{d\zeta} K^{-1}_{\zeta\zeta} \boldsymbol{K}_{\zeta d} \tag{2.34}$$

is the statically condensed element stiffness matrix. In terms of the integrals,

$$\tilde{\boldsymbol{K}}_{dd} = \int_{\Omega^e} \boldsymbol{B}^{\mathrm{t}} \boldsymbol{D}^{\mathrm{e}} \boldsymbol{G}\, \mathrm{d}\Omega^e \int_{\Omega^e} \boldsymbol{F}^{\mathrm{t}} \boldsymbol{D}^{\mathrm{e}} \boldsymbol{B}\, \mathrm{d}\Omega^e \Big/ \int_{\Omega^e} \left(\boldsymbol{F}^{\mathrm{t}} \boldsymbol{D}^{\mathrm{e}} \boldsymbol{G} + \tilde{\mathscr{H}}_\delta \right) \mathrm{d}\Omega^e. \tag{2.35}$$

For piecewise constant stress interpolations such as those arising from the use of 2D constant strain triangle (CST) and 3D tetrahedral elements, (2.35) simplifies to

$$\tilde{\boldsymbol{K}}_{dd} = \int_{\Omega^e} \boldsymbol{B}^{\mathrm{t}} \tilde{\boldsymbol{D}}^{\mathrm{p}} \boldsymbol{B}\, \mathrm{d}\Omega^e, \quad \tilde{\boldsymbol{D}}^{\mathrm{p}} = \frac{\boldsymbol{D}^{\mathrm{e}} \boldsymbol{G} \boldsymbol{F}^{\mathrm{t}} \boldsymbol{D}^{\mathrm{e}}}{\boldsymbol{F}^{\mathrm{t}} \boldsymbol{D}^{\mathrm{e}} \boldsymbol{G} + \tilde{\mathscr{H}}_\delta}. \tag{2.36}$$

Thus,

$$\tilde{\boldsymbol{K}} = \int_{\Omega^e} \boldsymbol{B}^{\mathrm{t}} \tilde{\boldsymbol{D}}^{\mathrm{ep}} \boldsymbol{B}\, \mathrm{d}\Omega^e, \quad \tilde{\boldsymbol{D}}^{\mathrm{ep}} = \boldsymbol{D}^{\mathrm{e}} - \tilde{\boldsymbol{D}}^{\mathrm{p}} \tag{2.37}$$

and so the equivalence of the standard Galerkin equation (2.24) with the assumed enhanced strain method presented in [16] is readily established for the case of piecewise constant stress interpolation.

Remark 2. From a constitutive modeling standpoint, it is enlightening to compare the deviatoric post-localization model adopted by Simo and co-workers [9,23–25] with the one considered in this paper. If the formulation of [9,23–25] were cast within the framework of the present formulation, then their post-localization model would not be the von Mises type but instead would be given by yield and plastic potential functions of the form

$$\mathscr{G} = \mathscr{R} = \boldsymbol{\sigma} : \mathrm{sym}(\boldsymbol{m} \otimes \boldsymbol{n}) - \tau_Y, \tag{2.38}$$

where $\boldsymbol{m}$ and $\boldsymbol{n}$ are orthogonal unit vectors determined from the bifurcation analysis, and τ_Y is the maximum resolved shear stress on the band. Eq. (2.38) defines a hyperplane in 6D stress space and has a form similar to the yield functions of crystal plasticity theory, where plastic deformations are restricted to glides on the well-defined crystallographic slip planes, see e.g., [31]. The stress gradients of (2.38) are constant and equal to

$$\frac{\partial \mathscr{G}}{\partial \boldsymbol{\sigma}} = \frac{\partial \mathscr{R}}{\partial \boldsymbol{\sigma}} = \mathrm{sym}(\boldsymbol{m} \otimes \boldsymbol{n}). \tag{2.39}$$

Substituting (2.39) in (2.27) gives

$$\tilde{\boldsymbol{\gamma}}^h = \xi \left[\frac{\ell^e_{\mathscr{S}}}{A_e} \mathrm{sym}(\boldsymbol{m} \otimes \boldsymbol{n}) - \mathrm{sym}(\boldsymbol{m} \otimes \boldsymbol{n}) \delta_{\mathscr{S}} \right], \tag{2.40}$$

thus, effectively capturing the weighting function used in [24,25]. Also, since $\tilde{\boldsymbol{\gamma}}^h$ is constant, (2.26b) can be replaced with the integrated equation

$$\int_{\Omega^e} \tilde{\boldsymbol{\gamma}}^h : (\boldsymbol{\sigma} - \boldsymbol{\sigma}^*)\, \mathrm{d}\Omega^e = 0 \quad \forall e \in \{\text{set of localized elements}\}, \tag{2.41}$$

where $\boldsymbol{\sigma}^*$ is the stress tensor at the onset of localization. In contrast, the post-localization model considered in the present paper allows a nonassociative response, with a general damage function $\mathscr{G}$ (as yet undefined) and a specific plastic potential function $\mathscr{R}$ given by the expression

$$\mathscr{R} = \boldsymbol{\sigma} : \mathrm{sym}(\boldsymbol{m} \otimes \boldsymbol{n}), \quad \frac{\partial \mathscr{R}}{\partial \boldsymbol{\sigma}} = \mathrm{sym}(\boldsymbol{m} \otimes \boldsymbol{n}), \tag{2.42}$$

where $\boldsymbol{m}$ and $\boldsymbol{n}$ now satisfy the relation $\boldsymbol{m} \cdot \boldsymbol{n} > 0$ for dilative response. Eq. (2.42) allows Eq. (2.9) to be captured identically by the present model. Clearly, the more robust formulation described in this paper allows more elaborate plasticity models to be incorporated into the post-localization theory.

3. Integration algorithm

As mentioned in the previous section the constant stress field considered in the standard CST finite element interpolation allows static condensation to be performed on the material level, and so the solution can be carried out using the standard Galerkin approximation. From a computational standpoint this is a significant advantage, since the static condensation technique is not as convenient to use in the nonlinear regime as the standard Galerkin approximation, which has well-developed algorithms that can be used neatly for nonlinear problems. The following section elaborates this point with a discussion of a stress-point integration algorithm for post-localization analysis borrowed from the ideas of classical computational plasticity.

3.1. General stress-point integration algorithm for post-localization analysis

The constitutive equation in rate form for a typical localized finite element e is given by

$$\dot{\boldsymbol{\sigma}} = \dot{\boldsymbol{\sigma}}^{\mathrm{tr}} - \dot{\zeta}^e \boldsymbol{c}^{\mathrm{e}} : \mathrm{sym}(\nabla f_e^h \otimes \boldsymbol{m}), \quad \dot{\boldsymbol{\sigma}}^{\mathrm{tr}} = \boldsymbol{c}^{\mathrm{e}} : \mathrm{sym}(\nabla \dot{\tilde{\boldsymbol{u}}}^h). \tag{3.1}$$

The first term on the right-hand side, $\dot{\boldsymbol{\sigma}}^{\mathrm{tr}}$, is the trial rate of stress obtained if the slip across the element is suppressed, while the second term represents the plastic flow correction due to the displacement jump across the element. The element dimensions and orientation enter into the continuum material response through the term ∇f_e^h. The element slip rate $\dot{\zeta}^e$ takes the role of the consistency parameter, while the tensor $\mathrm{sym}(\nabla f_e^h \otimes \boldsymbol{m})$ is analogous to the continuum plastic flow correction and reflects the equivalent unloading of the continuum in the neighborhood of the band as a result of the concentrated slip on the band.

The consistency condition on the band is provided by the rate equation

$$\frac{\partial \mathscr{G}}{\partial \boldsymbol{\sigma}} : \dot{\boldsymbol{\sigma}} - \tilde{\mathscr{H}}_\delta \dot{\zeta}^e = 0. \tag{3.2}$$

Eq. (3.2) guarantees that the stress point is yielding on the band. For a softening response on the band, $\dot{\zeta}^e > 0$ and $\tilde{\mathscr{H}}_\delta < 0$, and so $(\partial \mathscr{G}/\partial \boldsymbol{\sigma}) : \dot{\boldsymbol{\sigma}} < 0$, which means that the yield function $\mathscr{G}$ is contracting on the band. Simultaneous satisfaction of (3.1) and (3.2) guarantees that the stresses on the band are the same as those just outside the band.

The integration of (3.1) is straightforward and can be written in the incremental form as

$$\boldsymbol{\sigma}_{n+1} = \boldsymbol{\sigma}_{n+1}^{\mathrm{tr}} - \Delta\zeta^e \boldsymbol{c}^{\mathrm{e}} : \mathrm{sym}(\nabla f_e^h \otimes \boldsymbol{m}), \quad \boldsymbol{\sigma}_{n+1}^{\mathrm{tr}} = \boldsymbol{\sigma}_n + \boldsymbol{c}^{\mathrm{e}} : \mathrm{sym}(\nabla \tilde{\boldsymbol{u}}_{n+1}^h - \nabla \tilde{\boldsymbol{u}}_n^h), \tag{3.3}$$

where $\Delta\zeta^e$ is the incremental slip across the element. Assuming that $\tilde{\mathscr{H}}_\delta$ is constant, (3.2) can also be integrated in time to obtain

$$(\mathscr{G}_{n+1} - \mathscr{G}_n)_{\mathscr{A}} - \tilde{\mathscr{H}}_\delta \Delta\zeta^e = 0, \tag{3.4}$$

where $(\mathscr{G}_{n+1} - \mathscr{G}_n)_{\mathscr{A}}$ is the incremental change in the value of the yield function $\mathscr{G}$ due to changes in the stresses on the band with the plastic stress variable $\mathscr{A}$ of the yield function $\mathscr{G}$ held fixed. Note that (3.4) is the *exact* integral of (3.2).

The integration algorithm can now be phrased as follows. Given $\boldsymbol{\sigma}_n$, $\nabla\tilde{\boldsymbol{u}}^h_{n+1}$, ∇f^h_e, and $\boldsymbol{m}$, find $\boldsymbol{\sigma}_{n+1}$ such that (3.3) and (3.4) are satisfied. In addition to the stresses, the algorithm described above also allows the value of the incremental slip $\Delta\zeta^e$ to be determined. However, the solution must be done iteratively since the evolution equation for the yield function $\mathscr{G}$ is nonlinear in stresses. Let us solve this problem by Newton's method.

Putting (3.4) in residual form, we have

$$r(\Delta\zeta^e) = (\mathscr{G}_{n+1} - \mathscr{G}_n)_{\mathscr{A}} - \tilde{\mathscr{H}}_\delta \Delta\zeta^e. \tag{3.5}$$

The problem is to determine the value of $\Delta\zeta^e$ satisfying (3.3) that gives $r(\Delta\zeta^e) = 0$. Using Newton's method, we evaluate the consistent tangent operator as

$$-r'(\Delta\zeta^e) = \boldsymbol{b} : \boldsymbol{a} + \tilde{\mathscr{H}}_\delta, \tag{3.6}$$

where

$$\boldsymbol{a} = -\frac{\partial\boldsymbol{\sigma}_{n+1}}{\partial\Delta\zeta^e} = \boldsymbol{c}^{\mathrm{e}} : \mathrm{sym}(\nabla f^h_e \otimes \boldsymbol{m}), \quad \boldsymbol{b} = \frac{\partial\mathscr{G}_{n+1}}{\partial\boldsymbol{\sigma}_{n+1}}. \tag{3.7}$$

Note that the right-hand side of Eq. (3.6) is nothing else but the quantity χ defined in (2.24) and evaluated at time station t_{n+1}. By definition, this quantity must be positive, otherwise the incremental slip will be negative and the resulting solution is physically meaningless. If this requirement is satisfied, then the algorithm is well defined and the iteration for $\Delta\zeta^e$ can proceed in a standard fashion.

The next step is to determine the algorithmic tangential moduli tensor $\boldsymbol{c}_{n+1}$ consistent with the linearization of the update Eq. (3.3), which takes the form

$$\delta\boldsymbol{\sigma}_{n+1} = \boldsymbol{c}^{\mathrm{e}} : \delta\mathrm{sym}(\nabla\tilde{\boldsymbol{u}}^h_{n+1}) - \delta\zeta^e\boldsymbol{c}^{\mathrm{e}} : \mathrm{sym}(\nabla f^h_e \otimes \boldsymbol{m}). \tag{3.8}$$

Linearizing (3.4) gives

$$\frac{\partial\mathscr{G}_{n+1}}{\partial\boldsymbol{\sigma}_{n+1}} : \delta\boldsymbol{\sigma}_{n+1} = \tilde{\mathscr{H}}_\delta \delta\zeta^e. \tag{3.9}$$

Substituting (3.8) in (3.9) and simplifying, we obtain the algorithmic tangential moduli as

$$\boldsymbol{c}_{n+1} = \frac{\partial\boldsymbol{\sigma}_{n+1}}{\partial\mathrm{sym}(\nabla\tilde{\boldsymbol{u}}^h_{n+1})} = \boldsymbol{c}^{\mathrm{e}} - \frac{\boldsymbol{a}\otimes\tilde{\boldsymbol{a}}}{\boldsymbol{b}:\boldsymbol{a} + \tilde{\mathscr{H}}_\delta}, \tag{3.10}$$

where $\tilde{\boldsymbol{a}} = \boldsymbol{b} : \boldsymbol{c}^{\mathrm{e}}$. Interestingly, the algorithmic tangential moduli takes a form that is similar to that of the continuum elastoplastic tangential moduli, see (2.23). This latter point is noteworthy because it suggests that the update Eqs (3.3) and (3.4) are easily linearizable and therefore are amenable to efficient computer implementation.

As alluded to before, some restrictions apply to avoid numerical pathologies in Eq. (3.10). First, since $\boldsymbol{c}^{\mathrm{e}}$ is positive-definite, then we require that $\boldsymbol{b} : \boldsymbol{a} > 0$, which means that the gradient tensor $\boldsymbol{b}$ must be sufficiently "close" to the tensor $\mathrm{sym}(\nabla f^h_e \otimes \boldsymbol{m})$. If this is the case, then we can allow the softening parameter $\tilde{\mathscr{H}}_\delta$ to be less than zero since this is the condition of interest in the first place. However, we also require that $\tilde{\mathscr{H}}_\delta > -\boldsymbol{b} : \boldsymbol{a}$ in order for (3.10) to make sense. The aforementioned requirements are the same as those surrounding Eq. (2.24) and are discussed further below within the context of the CST finite element interpolation.

Figs. 3 and 4 show pictorially how ∇f^h is determined for a typical CST element crossed by a shear band. By definition, traced elements belong in the subdomain $\Omega^h = \Omega^h_- \cup \Omega^h_+$, as illustrated in Fig. 1, so all of their nodes belong to either $\mathscr{S}^h_-$ or to $\mathscr{S}^h_+$. A traced triangular element always contains a one-node side and a two-node side; clearly, if we adopt the element shape functions for f^h used in [23], then ∇f^h is always perpendicular to the two-node side. Referring to Fig. 4, $\boldsymbol{k}^e = (\boldsymbol{x}^* - \boldsymbol{x}_A)/h^e$ is the outward unit vector to the two-node side; hence, $\nabla f^h = \pm\boldsymbol{k}^e/h^e$, where the appropriate sign is chosen so that $\boldsymbol{n}\cdot\nabla f^h > 0$.

If the two-node side of a traced CST element is parallel to the shear band, then $\nabla f^h = \boldsymbol{n}/h^e$ and (2.24) reduces to

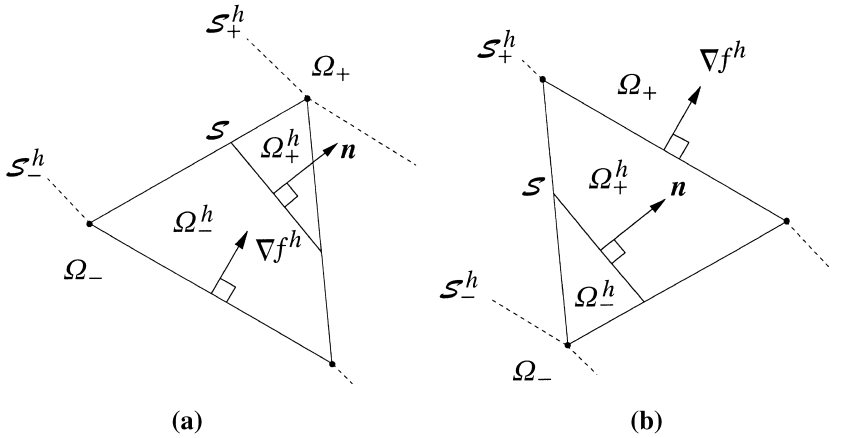

Fig. 3. CST elements crossed by a shear band: (a) one-node side on the positive side of $\mathscr{S}$ and (b) two-node side on the positive side of $\mathscr{S}$.

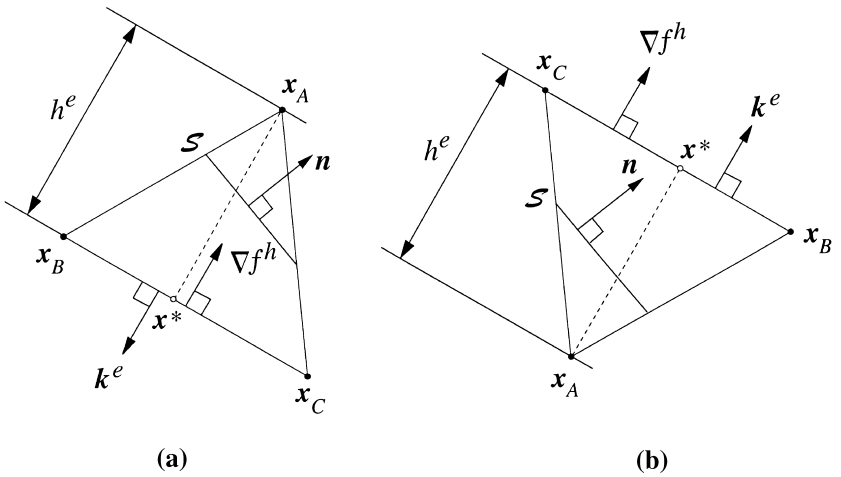

Fig. 4. Evaluation of ramp function gradient from CST element crossed by a shear band: (a) one-node side on the positive side of $\mathscr{S}$ and (b) two-node side on the positive side of $\mathscr{S}$.

$$\chi = \frac{1}{h^e}\boldsymbol{\psi} : \boldsymbol{c}^{\mathrm{e}} : \mathrm{sym}(\boldsymbol{n} \otimes \boldsymbol{m}) + \tilde{\mathscr{H}}_\delta. \tag{3.11}$$

The first term on the right-hand side of (3.11) is always positive for associative plasticity (post-localization definition, see Remark 2) due to the positive-definiteness of $\boldsymbol{c}^{\mathrm{e}}$, and so $\chi > 0$ provided that $\tilde{\mathscr{H}}_\delta > -\boldsymbol{\psi} : \boldsymbol{c}^{\mathrm{e}} : \mathrm{sym}(\boldsymbol{n} \otimes \boldsymbol{m})/h^e$. For nonassociative plasticity, a positive value for the first term on the right-hand side of (3.11) is not guaranteed unless $\boldsymbol{\psi}$ is sufficiently close to $\mathrm{sym}(\boldsymbol{n} \otimes \boldsymbol{m})$, such as the case for "mildly" nonassociated model. In this case, it is desirable to have a structured mesh in which the two-node side of a traced CST element is aligned to the shear band.

Fig. 5 shows a comparison between a well-traced CST element and a badly-traced element. The two elements are identical in both shape, orientation, and dimension, but the well-traced element of Fig. 5(a) has the shear band oriented approximately parallel to the two-node side, whereas the badly traced element of Fig. 5(b) has ∇f^h and $\boldsymbol{n}$ oriented almost perpendicular to each other. Note that although the exact position of the shear band within a traced element does not matter, the definition of which node belongs to what side, i.e., $\mathscr{S}_-^h$ or $\mathscr{S}_+^h$, does matter, and so the shear band in Fig. 5(b) cannot be arbitrarily moved to the left to obtain the more desirable condition shown in Fig. 5(a). This issue is elaborated further in the numerical examples discussed in Section 4.

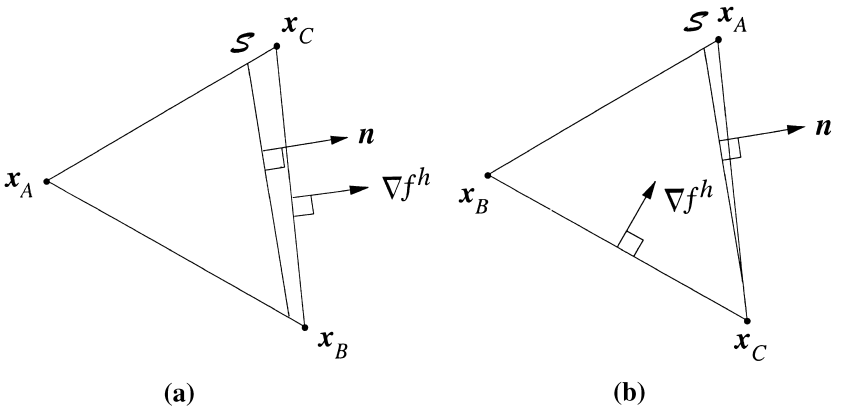

Fig. 5. Examples of traced elements: (a) well traced and (b) badly traced.

3.2. Specialization to nonassociated Drucker–Prager plasticity model

Let us now specialize the formulation to a nonassociated Drucker–Prager plasticity model. In this case, the yield function on the band is described by the equation

$$\mathscr{G} = \sqrt{\frac{3}{2}}\|\boldsymbol{s}\| + \sqrt{3}\beta p - \mathscr{A} = 0, \tag{3.12}$$

where

$$p = \frac{1}{3}\mathrm{tr}(\boldsymbol{\sigma}), \quad \boldsymbol{s} = \boldsymbol{\sigma} - p\mathbf{1} \tag{3.13}$$

and $\mathscr{A}$ is the size of the yield surface on the band which takes on the initial value

$$\mathscr{A}_0 = \sqrt{\frac{3}{2}}\|\boldsymbol{s}^*\| + \sqrt{3}\beta p^*, \tag{3.14}$$

where $\boldsymbol{s}^*$ and p^* are the respective values of $\boldsymbol{s}$ and p at the onset of localization. The frictional component of the yield function is represented by the material parameter β, and the plastic potential function $\mathscr{R}$ at post-localization is given by (2.39). The size $\mathscr{A}$ of the yield function is assumed to vary with the slip parameter ζ through the softening modulus $\tilde{\mathscr{H}}_\delta$.

For this nonassociated model, we have

$$\frac{\partial \mathscr{G}}{\partial \boldsymbol{\sigma}} : \dot{\boldsymbol{\sigma}} = \sqrt{\frac{3}{2}}\frac{\boldsymbol{s} : \dot{\boldsymbol{s}}}{\|\boldsymbol{s}\|} + \sqrt{3}\beta\dot{p}. \tag{3.15}$$

Noting that $\boldsymbol{s} : \mathrm{d}\boldsymbol{s} = \mathrm{d}\|\boldsymbol{s}\|^2/2$, we get

$$(\mathscr{G}_{n+1} - \mathscr{G}_n)_{\mathscr{A}} = \sqrt{\frac{3}{2}}(\|\boldsymbol{s}_{n+1}\| - \|\boldsymbol{s}_n\|) + \sqrt{3}\beta(p_{n+1} - p_n), \tag{3.16}$$

which is the exact integral of the consistency condition (2.20).

The criterion for numerical stability is (2.24), which specializes for the nonassociated Drucker–Prager model to

$$\chi = 2\mu\sqrt{\frac{3}{2}}\frac{\boldsymbol{s}}{\|\boldsymbol{s}\|} : \mathrm{sym}(\nabla f^h \otimes \boldsymbol{m}) + \sqrt{3}K\beta(\nabla f^h \cdot \boldsymbol{m}) + \tilde{\mathscr{H}}_\delta > 0. \tag{3.17}$$

If the two-node side of a traced CST element is aligned to the shear band, then $\nabla f^h = \boldsymbol{n}/h^e$, and (3.17) simplifies to

$$\chi = \frac{2\mu}{h^e}\sqrt{\frac{3}{2}}\frac{\boldsymbol{s}}{\|\boldsymbol{s}\|} : \mathrm{sym}(\boldsymbol{n}\otimes\boldsymbol{m}) + \sqrt{3}K\frac{\beta}{h^e}(\boldsymbol{n}\cdot\boldsymbol{m}) + \tilde{\mathscr{H}}_\delta > 0. \tag{3.18}$$

But $\boldsymbol{n}\cdot\boldsymbol{m} > 0$ for dilatant behavior, and $\boldsymbol{s} : \mathrm{sym}(\boldsymbol{n}\otimes\boldsymbol{m}) > 0$ can easily be satisfied by appropriately choosing the signs of $\boldsymbol{n}$ and $\boldsymbol{m}$ at the onset of localization, so here, we see again that if the two-node sides of the traced CST elements are sufficiently aligned to the shear band, then the necessary condition that the incremental slip be positive is guaranteed for "mild" values of $\tilde{\mathscr{H}}_\delta$.

4. Numerical examples

In this section we present two numerical examples, the first involving simple shearing of elastoplastic solids with deviatoric plastic flow, and the second involving plane strain compression of dilatant cohesive/frictional materials, to demonstrate objectivity with respect to mesh refinement and insensitivity to mesh alignment of finite element solutions employing the proposed Galerkin formulation. In order for the comparison of the solutions to be meaningful, it is necessary that the standard finite element solutions provided by the different meshes prior to localization be the same, otherwise the onset of localization will be a function of the accuracy of the finite element meshes and an objective comparison of the different solutions could be difficult.

The procedure followed in the analyses goes as follows. First, different meshes are constructed for a structure deforming homogeneously. This guarantees that all the elements will localize at the same time, which in turn implies that the initiation of the bifurcated response will take place at the same stress state regardless of the mesh. No weak elements were introduced, and no specific band tracing algorithm was employed other than the fact that all the elements on a potential shear band were assumed to localize simultaneously. Since the structure is initially deforming homogeneously, there is theoretically an infinite number of potential shear bands that could form, and one of them is chosen a priori with the requirement that the band is able to develop completely by not making it pass through a constrained boundary of the structure. The ultimate goal of the analyses is to show that the bifurcated responses exhibited by the various finite element solutions are not only the same but are *numerically identical to machine precision*, regardless of the mesh. Details of the solutions are given in the individual examples that follow.

4.1. Simple shearing on elastoplastic solid with deviatoric plastic flow

The structure consists of a rectangular solid 5 m long and 1 m tall, and deforming in plane strain as depicted in Fig. 6. Three finite element meshes are constructed for this problem: two are regular/structured with different degrees of refinement, and a third is an irregular mesh in which none of the element sides is oriented parallel to the potential shear band. The base of the structure is pinned to fixed supports, while the top of the structure is pinned to supports that move uniformly rightward in the horizontal direction. Horizontal roller supports are provided on the left and right vertical sides of the meshes to avoid end effects and thus guarantee homogeneous deformation prior to localization. Prior to localization, the material is assumed to obey the von Mises yield criterion with associative flow rule, with Young's modulus $E =$ 26,000 kPa; Poisson's ratio $\nu = 0.30$; and yield stress in simple shear $\tau_Y = 20$ kPa. Since the elastic shear modulus is $\mu = 10{,}000$ kPa, the engineering shear strain at initial yield can be computed as $\gamma_Y = \tau_Y/\mu = 0.002$, which implies that the solid will yield when the upper boundary has moved by a horizontal distance of $\delta = 0.002$ m.

For von Mises yield criterion with associative flow rule the localization condition for plane strain deformation is $s_3 = 0$, where s_3 is the normal off-plane component of the deviatoric stress tensor $\boldsymbol{s}$ [16,32]. For the case of simple shearing the condition $s_3 = 0$ is identically satisfied right at initial yielding; hence, a bifurcated response is possible right at the onset of yielding. Two potential types of shear band have been identified: a horizontal shear band with $\boldsymbol{n} = (0,1,0)$, and a vertical shear band in which $\boldsymbol{n} = (1,0,0)$. The former orientation is chosen from the criterion that $\nabla\boldsymbol{u} : (\boldsymbol{m}\otimes\boldsymbol{n})$ be maximum, where $\boldsymbol{u}$ is the instantaneous

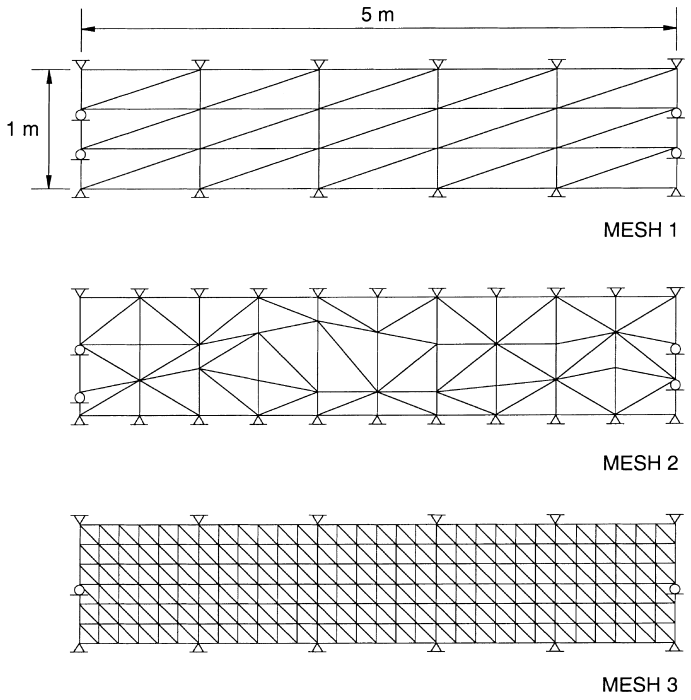

Fig. 6. Plane strain shear test on von Mises material with deviatoric flow: finite element meshes.

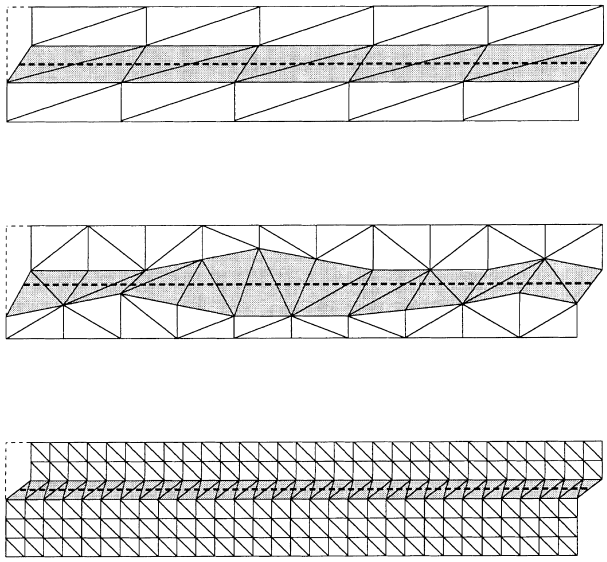

Fig. 7. Deformed meshes for plane strain shear test: shaded regions denote localized elements (displacement magnification = 50).

displacement field of the continuum at the onset of localization [16]. The eigenvector resulting from the singular solution yields $\boldsymbol{m} = (1, 0, 0)$, which gives $\boldsymbol{m} \cdot \boldsymbol{n} = 0$.

The deformed meshes are shown in Fig. 7. All localized elements, including the irregular ones, satisfy the criterion for nonnegative slip, (2.24), which resulted in the solutions progressing successfully to completion. As demonstrated in Fig. 7, the shear bands (represented by dashed lines) are resolved sharply across the traced elements (shaded gray). The shear force–shear displacement curves are plotted in Fig. 8 for the cases $\tilde{\mathscr{H}}_\delta = -5{,}000$ kPa and $\tilde{\mathscr{H}}_\delta = -2{,}600$ kPa. In both the cases, the post-localization solutions provided by all the meshes are numerically identical to machine precision.

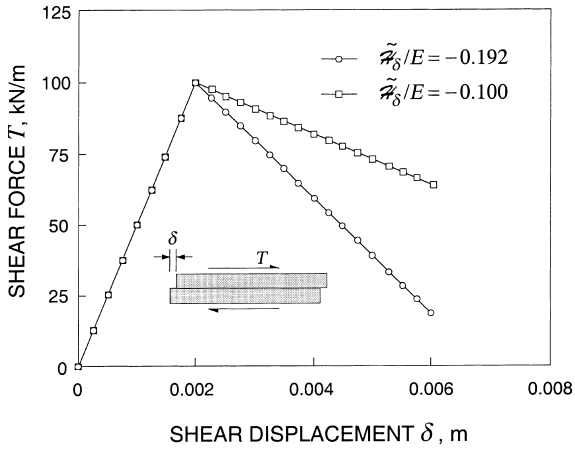

Fig. 8. Force–displacement relation for plane strain shear test with localization mode and deviatoric plastic flow.

4.2. Plane strain compression of dilatant cohesive/frictional material

The structure consists of a rectangular medium 1 m wide and 3 m tall and deforming in plane strain, as shown in Fig. 9. Three meshes were considered initially for the analysis: a 150-element regular/unstructured mesh, an 81-element irregular mesh, and a 900-element regular/structured mesh in which the element sides are aligned to the shear band. Both the top and base of the specimen are supported on horizontal rollers, but the vertical motion at the base is restricted to zero while the motion at the top is prescribed to produce vertical compression.

The material response is modeled by a nonassociated elastoplastic Drucker–Prager yield criterion with $E = 20,000$ kPa, $\nu = 0.40$, $\beta = 0.495$, $b = 0.300$, and $\alpha_0 = 17.143$ kPa (see [16] for the physical meanings of these model parameters). The last three parameters are equivalent to having an initial cohesion of $c = 20$ kPa, a friction angle of $\phi = 30°$, and a dilatancy angle of $\psi = 16.53°$. The hardening modulus prior to localization is taken as $H' = 100$ kPa. For plane strain compression in which the exposed vertical sides on

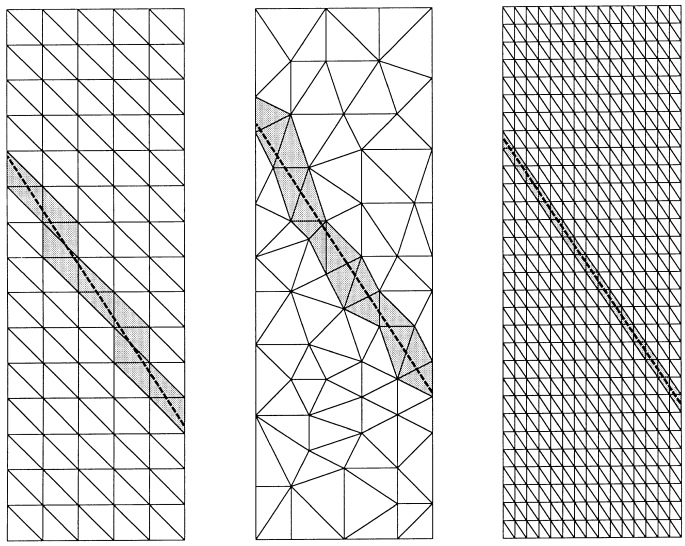

Fig. 9. Plane strain compression of nonassociated Drucker–Prager material with localization mode. Dashed lines denote potential shear band traced through shaded elements: (a) regular/unstructured grid; (b) irregular grid and (c) fine/structured grid.

the plane of deformation are free of traction, the localization condition is given in [16,32] and occurs when the vertical stress is $\sigma_v = -74.9$ kPa and the normal off-plane stress is $\sigma_3 = -45.7$ kPa.

The continuum solution prior to localization results in a symmetric displacement gradient $\nabla \boldsymbol{u}$ that does not allow the determination of a unique shear band orientation from two possible orientations. By choice, one of the two orientations is considered in Fig. 9. By the procedure described in [16,32], the shear band orientation is determined to be equal to 56.44° relative to the horizontal axis. Note that this orientation is closer to $45° + (\phi + \psi)/4 = 56.63°$, as suggested in [33], than to either $45° + \phi/2 = 60°$ or to $45° + \psi/2 = 53.26°$, and demonstrates the influence of both the friction angle ϕ and dilatancy angle ψ on the final orientation of the shear band [34,35]. From the eigenvalue analysis we obtain the corresponding eigenvector $\boldsymbol{m}$, from which we compute $\boldsymbol{m} \cdot \boldsymbol{n} = 0.321$, or $\psi^* = \sin^{-1}(0.321) = 18.7°$, where ψ^* is the angle that $\boldsymbol{m}$ makes with respect to the shear band at onset of localization [16]. The angle ψ^* at the point of localization is slightly higher than the continuum dilatancy angle ψ but is lower than the friction angle ϕ. For clarity, the angle ψ^* is assumed constant throughout the post-localization analysis.

Having defined the shear band, numerical analyses were then carried out beyond the point of bifurcation using the proposed finite element procedure. Fig. 10 shows the deformed meshes demonstrating sharp resolution of the discontinuity. Observe the marked dilatancy within the localized elements (shaded gray) exhibited by the finite element solutions. Again, the modes of deformation are practically identical in all the three cases, and all the solutions progressed to completion in four iterations or less per load step.

The fact that the solutions have progressed to completion indicates that no element has been traced poorly in any of the three cases, not even in the regular/unstructured grid of Figs. 9(a) and 10(a) where the localized elements have been traced in a ladder-like manner to accommodate a steeper shear band orientation. This point is further corroborated pictorially in Fig. 11 which shows three-dimensional perspective views of the ramp function f^h suggesting how the gradient ∇f^h might have affected the numerical conditioning of the post-localization solutions. The ideal condition would be to have the structured mesh of Fig. 11(c) where ∇f^h crosses the shear band at right angles; however, even the unstructured and regular meshes of Figs. 11(a) and (b) have been accommodated very well by the model, resulting in identical localized modes (Fig. 10) which literally can be placed one on top of the other.

As an example of how the numerical conditioning of the problem can corrupt the stability of the numerical solution, we consider a mesh with diamond pattern shown in Fig. 12. Here, the shear band traces four elements poorly, two in the middle of the mesh and two on the sides, represented by sad faces in Fig. 12(a). All the four elements violated the nonnegative slip criterion at the onset of localization,

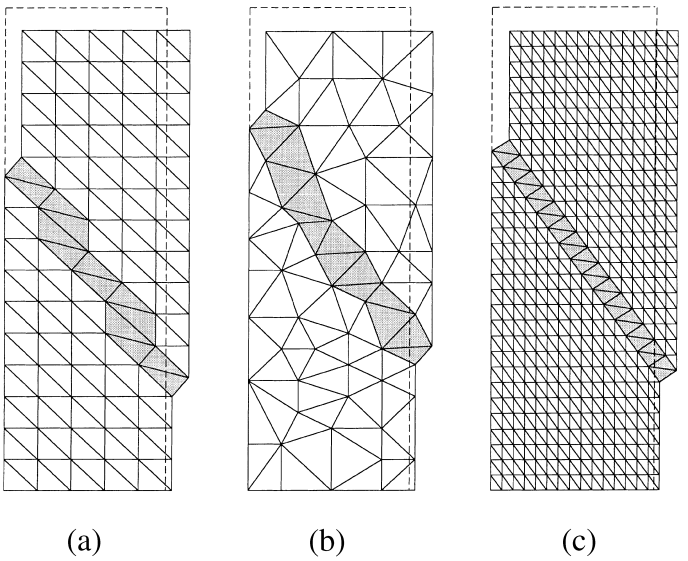

Fig. 10. Deformed meshes for plane strain compression example: (a) regular/unstructured grid; (b) irregular grid and (c) fine /structured grid (displacement magnification = 4).

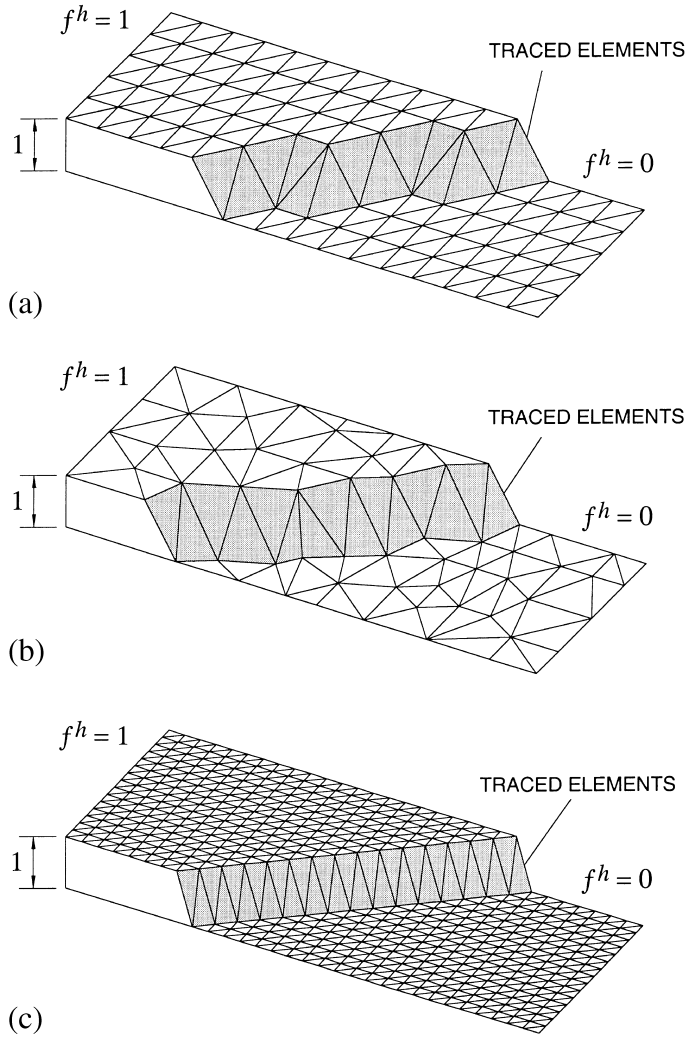

Fig. 11. Ramp functions for plane strain compression example: (a) regular/unstructured grid; (b) irregular grid and (c) fine/structured grid.

Eq. (2.24), resulting in the solutions failing to continue beyond the point of localization. Fig. 12(b) shows how the problem has been eliminated by a simple adjustment of the coordinates of the nodes defining the problem elements. The idea is to reduce the angle between ∇f^h and $\boldsymbol{n}$ by adjusting the coordinates of the two-node sides of the problem triangles. Using the modified grid of Fig. 12(b), the solution has been carried out to completion resulting in the deformed mesh shown in Fig. 12(c).

To further elaborate the idea of circumventing the problem associated with badly traced elements, Fig. 13 compares the ramp functions f^h for the original and modified meshes of Figs. 12(a) and (b), respectively. The ramp function for the original mesh is so badly distorted that a sharp resolution of the shear band is inhibited, thus preventing the solution to finish successfully. However, by slightly adjusting the nodal coordinates, the distortion in the ramp function has been reduced to such an extent that the problem of numerical ill-conditioning is completely eliminated, as shown in Fig. 13(b). Again, it must be noted that the ramp function f^h is not meant to approximate the Heaviside function $H_{\mathscr{S}}$ since (2.16) shows that $M_{\mathscr{S}}$, combined with the function f^h, always results in the exact jump function $H_{\mathscr{S}}$.

Fig. 14 shows the force–displacement relations for the plane strain compression problem using three different values of the softening modulus $\tilde{\mathscr{H}}_\delta$: $-1,000$, -500, and -300 kPa. As in Example 4.1, all of the meshes of Fig. 9, as well as the modified mesh of Fig. 12(b), yield numerically identical force–displacement

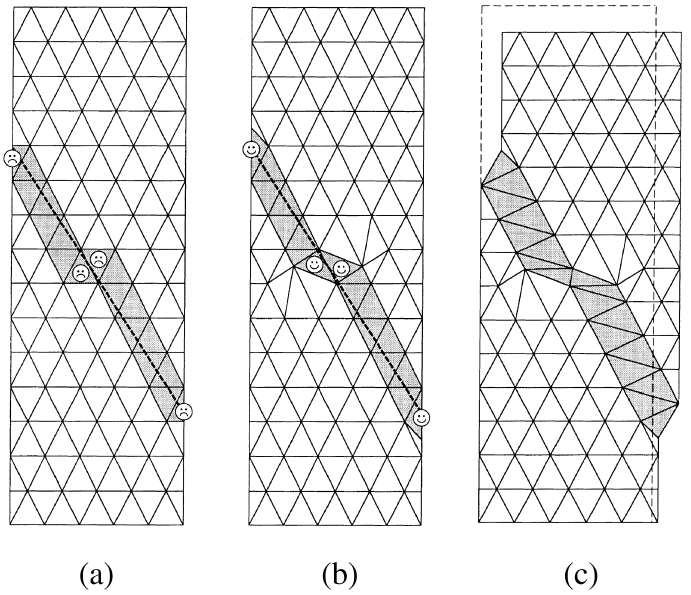

Fig. 12. Finite element mesh with diamond pattern for plane strain compression example: (a) original grid; (b) modified grid and (c) deformed mesh.

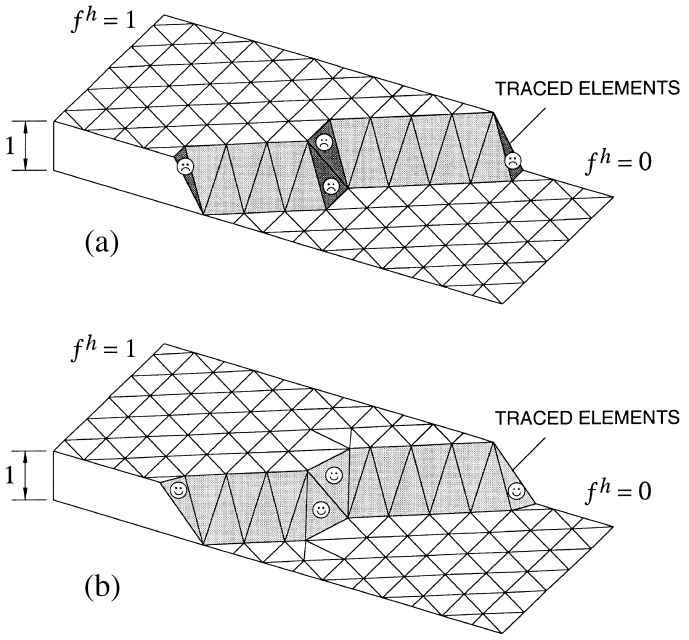

Fig. 13. Ramp functions for mesh with diamond pattern: (a) original grid and (b) modified grid.

relations to machine precision. Observe that the exact integration of the stresses at post-localization results in force–displacement curves that taper vertically with degree of softening, i.e. the post-localization curves are not straight lines even if $\tilde{\mathscr{H}}_\delta$ is constant. This is because the direction of the gradient tensor $\boldsymbol{\psi} = \partial \mathscr{G}/\partial \boldsymbol{\sigma}$ in (2.21) varies with the degree of softening for the plane strain compression problem (mainly induced by the normal off-plane stress component due to Poisson's ratio effect), unlike in the simple shear problem of Example 4.1, where the direction of $\boldsymbol{\psi}$ is constant, and hence, the post-localization relation is a simple straight line (see Fig. 8).

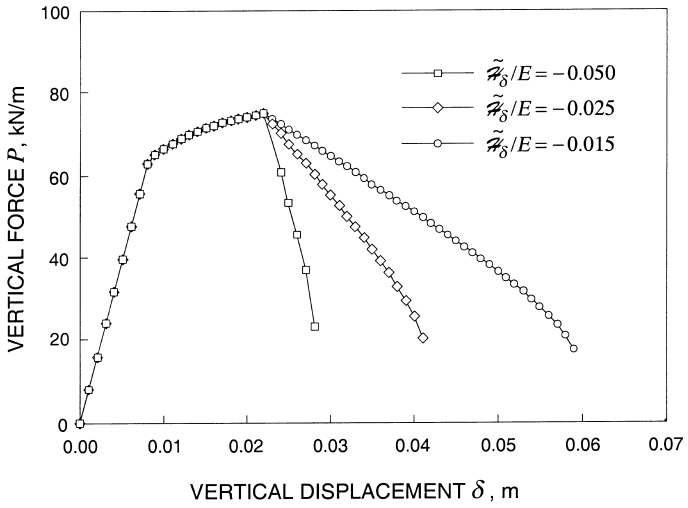

Fig. 14. Force–displacement relation for plane strain compression test on Drucker–Prager material with localization mode and nonassociated plastic flow.

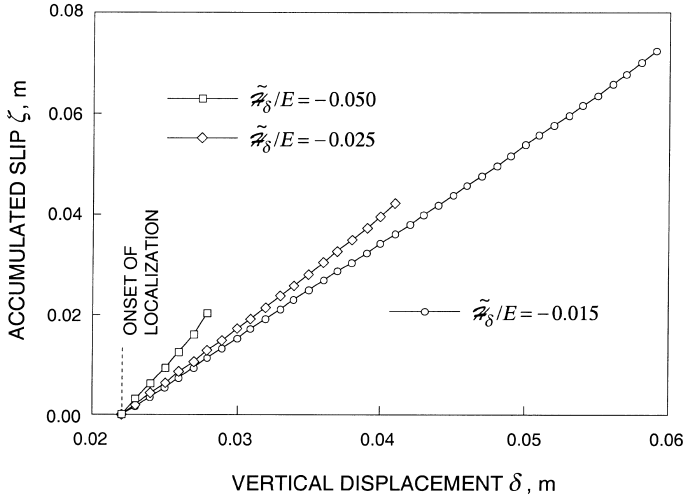

Fig. 15. Slip magnitude–displacement relation for plane strain compression test on Drucker–Prager material with localization mode and nonassociated plastic flow.

Finally, Fig. 15 shows the accumulated slip-vertical displacement relation for the plane strain compression example. Again, the displacement jumps are uniform across the traced elements, and their values are exact to machine precision regardless of the mesh. Like Fig. 14, the relationship between the accumulated slip magnitude ζ and the vertical displacement δ at the top boundary is not a straight line, but this time the curves slightly taper upwards. For clarity, we recall that the total displacement jump vector across $\mathscr{S}$ is $[\![\boldsymbol{u}]\!] = \zeta \boldsymbol{m}$, with ζ representing the magnitude of this jump. Since $\boldsymbol{m}$ and $\boldsymbol{n}$ are assumed constant at post-localization from their values at the onset of localization, the tangential component of the jump can be readily evaluated as $\zeta \cos\psi^*$, while the normal component is $\zeta \sin\psi^*$, where $\psi^* = \sin^{-1}(\boldsymbol{m} \cdot \boldsymbol{n})$.

Remark 3. *Why the standard Galerkin approximation works.* Apart from the established equivalence with the assumed enhanced strain method discussed in Section 2.3, the Galerkin approximation advocated in this paper works because the material subroutine uses a consistent vector quantity ∇f^h to extract information on the orientation and dimension of the localized elements. From the point of view of the material

routine, this is all the information it needs to provide an objective, mesh-independent solution to the problem of localization of deformation arising from jumps in the displacement field. The fact that the post-localization solution can be carried out in a standard Galerkin approach is a significant simplification since it allows practically all the attributes of robust plasticity algorithms to be carried over to the post-localization regime with very little modification.

5. Summary and conclusion

A finite element model for strain localization analysis of elastoplastic solids subjected to discontinuous displacement fields has been presented. The formulation is based on standard Galerkin approximation revolving around the dual response of a macroscopic point crossed by a shear band, which requires the satisfaction of the yield condition on the band as the same stress point unloads elastically just outside the band. Strain enhancements via jumps in the displacement field are captured and condensed on the material level, leading to a formulation that does not require static condensation to be performed on the element level. The post-localization stress-point integration algorithm is exact and amenable to consistent linearization. Numerical examples involving simple shearing of elastoplastic solids with deviatoric plastic flow and plane strain compression of dilatant cohesive/frictional materials demonstrate objectivity of the model with respect to mesh refinement and insensitivity of the finite element solutions to mesh alignment. Possible numerical ill-conditioning due to badly-traced elements has been discussed, as well as simple ways to circumvent and even completely eliminate this problem.

Acknowledgements

The work presented in this paper was supported by the G3S Division of the National Science Foundation through Grant No. CMS97-00426 under the directorship of Dr. Priscilla P. Nelson. This support is greatly acknowledged.

References

[1] T.W. Lambe, R.V. Whitman, Soil Mechanics, Wiley, New York, 1969.
[2] M.J. Hvorslev, Physical components of the shear strength of saturated clays, Research Conference on Shear Strength of Cohesive Soils, ASCE, June 1960, pp. 169–273.
[3] K.H. Roscoe, The influence of strains in soil mechanics, 10th Rankine Lecture, Géotechnique 20 (2) (1970) 129–170.
[4] G. Scarpelli, D.M. Woods, Experimental observations of shear band patterns in direct shear tests, in: Proceedings IUTAM Conference on Deformation and Failure of Granular Materials, Delft, Balkema Publ., Rotterdam, 1982, pp. 473–484.
[5] W. Johnson, Henri Tresca as the originator of adiabatic heat lines, Int. J. Mech. Sci. (1987) 301–310.
[6] R.J. Hill, J.W. Hutchinson, Bifurcation phenomena in the plane tension test, J. Mech. Phys. Solids 23 (1975) 239–264.
[7] J.W. Rudnicki, J.R. Rice, Conditions for the localization of deformation in pressure sensitive dilatant materials, J. Mech. Phys. Solids 23 (1975) 371–394.
[8] J.R. Rice, The localization of plastic deformation, in: W.T. Koiter (Ed.), Theoretical and Applied Mechanics, North Holland, Amsterdam, 1976, pp. 207–220.
[9] J.C. Simo, J. Oliver, F. Armero, An analysis of strong discontinuities induced by strain-softening in rate-independent inelastic solids, Comput. Mech. 12 (1993) 277–296.
[10] N. Triantafyllidis, E.C. Aifantis, A gradient approach to localization of deformation, I: Hyperelastic materials, J. Elasticity 16 (1986) 225–237.
[11] R. de Borst, L.J. Sluys, Localisation in a Cosserat continuum under static and dynamic loading conditions, Comput. Methods Appl. Mech. Engrg. 90 (1991) 805–827.
[12] Z.P. Bazant, M. Belytschko, T.P. Chang, Continuum theory for strain-softening, J. Engrg. Mech., ASCE 110 (1984) 1666–1691.
[13] B.D. Coleman, M.L. Hodgon, On shear bands in ductile materials, Arch. Rat. Mech. Anal. 90 (1985) 219–247.
[14] B. Loret, J.H. Prevost, Dynamic strain localization in elasto-(visco-)plastic solids, Part 1. General formulation and one-dimensional examples, Comput. Methods Appl. Mech. Engrg. 83 (1990) 247–273.
[15] J.H. Prevost, B. Loret, Dynamic strain localization in elasto-(visco-)plastic solids, Part 2. Plane strain examples, Comput. Methods Appl. Mech. Engrg. 83 (1990) 275–294.
[16] R.I. Borja, R.A. Regueiro, Strain localization in frictional materials exhibiting displacement jumps, Comput. Methods Appl. Mech. Engrg., in press.

[17] C.A. Coulomb, Essai sur une application des règles de Maximus et Minimis à quelques Problèmes de Statique, relatifs à l'Architecture, Mémoires de Mathématique et de Physique, Présentés a l'Académie Royale des Sciences, par divers Savans, et lûs dans ses Assemblées, Paris 7 (1776) 343–382.
[18] W.J.M. Rankine, On the stability of loose earth, Philos. Trans. Roy. Soc. London 147 (1) (1857) 9–27.
[19] K. Terzaghi, Theoretical Soil Mechanics, Wiley, New York, 1943.
[20] G.G. Meyerhof, The ultimate bearing capacity of foundations, Géotechnique 2 (1951) 301–332.
[21] A.W. Bishop, The use of the slip circle in the stability analysis of earth slopes, Géotechnique 5 (1955) 7–17.
[22] N. Janbu, L. Bjerrum, B. Kjaernsli, Veiledning ved losing av fundamenteringsoppgaver, Norwegian Geotechnical Institute Publisher, Oslo, 16, 1956.
[23] J.C. Simo, J. Oliver, A new approach to the analysis and simulation of strain softening in solids, in: Z.P. Bazant, Z. Bittnar, M. Jirásek, J. Mazars (Eds.), Fracture and Damage in Quasibrittle Structures, E&FN Spon, vol. 2–6 Boundary Row, London 1994, pp. 25–39.
[24] F. Armero, K. Garikipati, Recent advances in the analysis and numerical simulation of strain localization in inelastic solids, in: D.R.J. Owen, E. Oñate, E. Hinton (Eds.), Proceedings of the Computational Plasticity IV, CIMNE, Barcelona, Spain, 1995, pp. 547–561.
[25] K.R. Garikipati, On Strong Discontinuities in Inelastic Solids and Their Numerical Simulation, Ph.D. Thesis, Stanford University, Stanford, California, 1996.
[26] R. Larsson, K. Runesson, S. Sture, Embedded localization band in undrained soil based on regularized strong discontinuity theory and FE analysis, Int. J. Solids Struc. 33 (1996) 3081–3101.
[27] R. Larsson, K. Runesson, N.S. Ottosen, Discontinuous displacement approximation for capturing plastic localization, Int. J. Numer. Methods Engrg. 36 (1993) 2087–2105.
[28] J. Oliver, M. Cervera, O. Manzoli, On the use of J_2 plasticity models for the simulation of 2D strong discontinuities in solids, in: D.R.J. Owen, E. Hinton (Eds.), Computational Plasticity Fundamentals and Applications, CIMNE, Barcelona, 1997, pp. 38–55.
[29] J.C. Simo, M.S. Rifai, A class of mixed assumed strain methods and the method of incompatible modes, Int. J. Numer. Methods Engrg. 29 (1990) 1595–1638.
[30] I. Stakgold, Green's Functions and Boundary Value Problems, second Ed., Wiley, New York, 1998.
[31] R.I. Borja, J.R. Wren, Discrete micromechanics of elastoplastic crystals, Int. J. Numer. Methods Engrg. 36 (1993) 3815–3840.
[32] K. Runesson, D. Peric, S. Sture, Discontinuous bifurcations of elastic-plastic solutions at plane stress and plane strain, Int. J. Plasticity 7 (1991) 99–121.
[33] J.R.F. Arthur, T. Dunstan, Q.A.L.J. Al-ani, A. Assadi, Plastic deformation and failure in granular media, Géotechnique 27 (1977) 53–74.
[34] P.A. Vermeer, R. de Borst, Nonassociated plasticity for soils, concrete and rock, Heron 29 (1984) 1–64.
[35] I. Vardoulakis, B. Graf, Calibration of constitutive models from granular materials from data from biaxial experiments, Géotechnique 35 (1985) 299–317.